(Received 10 May 2025, Accepted 23 June 2025, Scheduled 19 July 2025)

Vibration Suppression Control of PMa-BSynRM Based on Variable Step Size and Variable Angle Search Algorithm

Jing Lu[1], Tengfei Zhao[2,*], and Huangqiu Zhu[2,*]

[1] School of Electrical Engineering, Southeast University, Nanjing 210096, China
[2] School of Electrical and Information Engineering, Jiangsu University, Zhenjiang 212013, China

ABSTRACT: The unbalanced rotor mass of permanent magnet assisted bearingless synchronous reluctance motor (PMa-BSynRM) will cause rotor vibration at the same frequency, which has a great influence on its operating performance at high speed. To solve this problem, a control method of unbalance vibration suppression based on variable step size and variable angle search algorithm is proposed in this paper. Firstly, the causes of rotor vibration are analyzed, and the equations of motion of the rotor in vibratory state are derived. Secondly, the improved Sigmoid function is used to change the step size and angle of the search algorithm, and a fuzzy inference machine is used to adjust the Sigmoid function weights. The vibration suppression control system is constructed, and vibration suppression simulation is performed. The vibration suppression control of the PMa-BSynRM is realized. Finally, the PMa-BSynRM experimental platform is established, and vibration suppression experiments are carried out under the conditions of equal speed and external interference. Experimental results show that the control algorithm can effectively suppress rotor vibration. The unbalanced vibration suppression control proposed in this paper can achieve stable levitation operation of the PMa-BSynRM.

1. INTRODUCTION

In the last 10 years, magnetic bearings benefit from the development of power electronics technology and have a wide range of applications. They have the advantages of no lubrication, no friction and wear, high rotational speed, high precision, etc., and are more suitable for applications in complex environments and widely used in semiconductor and bioengineering fields that require dust-free operation, and in aerospace fields that require high speed and high precision. Therefore, magnetic bearings and non-contact bearings using magnetic levitation technology have become one of the current research hotspots [1, 2].

Bearingless motor has two sets of windings stacked in the stator. They interact with each other to make bearingless motor rotate and suspend at the same time. When running at high speed, there is no mechanical contact between the stator and rotor, so there will be no friction and wear, and no need for lubrication. The efficiency and service life of the motor will be greatly improved. Compared with magnetic bearing system, bearingless motor system has shorter axial length, relatively simple structure, and low cost. The permanent magnet assisted bearingless synchronous reluctance motor (PMa-BSynRM) is a new type of bearingless motor [3], in which permanent magnets are embedded in the rotor multi-layer magnetic barrier of the bearingless synchronous reluctance motor to assist the excitation and improve the torque density of the motor. PMa-BSynRM has advantages of no friction and wear, high precision, no lubrication, high critical speed, high torque density, and long service life, etc., which make it have a wide application prospect in semiconductor industry, chemical industry, biopharmaceutical, transportation, aerospace, etc. [4, 5].

In engineering applications, due to machining errors and unbalanced materials used, the center of mass and the geometric center of the rotor of the PMa-BSynRM do not coincide with each other, which causes the rotor dynamic eccentricity, and an unbalanced force is generated during the rotation of the rotor, resulting in unbalanced vibration of the rotor system. The unbalance vibration suppression technology is the key to realize the stable operation of PMa-BSynRM system. In order to improve rotor vibration, various rotor vibration suppression schemes have been proposed in large number of literatures

Magnetic suspension rotor unbalanced vibration suppression control can be divided into bearing electromagnetic force minimum control and rotor displacement minimum control. Among them, the bearing electromagnetic force minimum control is to filter the unbalanced vibration signal in the feedback signal by filtering technology, reduce the amplitude of the unbalanced vibration signal, and make the rotor rotate around its inertia axis as much as possible. Generally, the generalized notch method and leastmeansquare (LMS) algorithm are used to control the unbalance force of the rotor and reduce the homogeneous frequency vibration of the rotor. The rotor displacement minimization control is to increase the control current through certain measures or compensation algorithms and enhance the active control of magnetic bearings, so that the rotor rotates as much as possible around its geometrical centre [6, 7]. In [8], in order to suppress the unbalanced vibration of a four-degree-of-freedom six-pole hybrid magnetic bearing rotor, a feed-forward compensation control strategy for rotor vibration based on vari-

* Corresponding authors: Tengfei Zhao (2222207109@stmail.ujs.edu.cn); Huangqiu Zhu (zhuhuangqiu@ujs.edu.cn).

able step size LMS adaptive filtering is proposed. In [9], the unbalance vibration of the active magnetic bearing rotor is weakened by notch filtering to achieve stable operation of the rotor in the full speed domain. In [10], an adaptive filtering algorithm based on recursive least square (RLS) method is used to extract synchronous vibration signals and completes vibration suppression control of active magnetic bearing rotor system through feedforward compensation. In [11] to address the vibration problem caused by rotor unbalance in PMa-BSynRM, a feedforward closed-loop suppression control scheme based on TLS adaptive filtering algorithm is proposed. Based on the improved notch filter, a method to suppress synchronous unbalance vibration in the finite iterative optimization process by using variable angle compensation algorithm is proposed in [12], which directly realizes real-time rotor vibration suppression control.

Modern control theory applied to magnetic suspension rotor system can also realize rotor vibration suppression [13, 16]. In [13], a basic acceleration feedforward compensation (BAFC) algorithm is proposed, which uses online basic excitation data and the dynamic model of the rotor system to determine the optimal compensation current in real time. In [14], a fuzzy controller is used to adjust controller bandwidth and observer bandwidth to realize fuzzy control and enhanced linear active disturbance rejection control of bearingless induction motor. In [15], an adaptive sliding mode controller for hybrid magnetic bearing (HMB) system is proposed, which can achieve the active axial position control of the HMB system, improve the robustness of the system, and effectively reduce rotor vibration. In [16], a three-vector model is proposed to predict suspension force control method. The simulated and experimental results verify that this method can effectively improve the control accuracy of BPMSM, thereby reducing rotor vibration and stabilizing the suspension of the rotor. The controller design based on modern control theory is more complicated and will be affected by the accuracy of mathematical model, which is not conducive to the unbalance vibration suppression of the PMa-BSynRM system. Therefore, in practical applications, the commonly adopted method is feed-forward suppression control by synchronous vibration signal detection.

In this paper, a variable step size and variable angle search algorithm based on a fuzzy inference system is proposed for the unbalanced vibration control of PMa-BSynRM rotor. The algorithm transforms the rotor vibration problem into a problem of solving the equivalent unbalance coefficient. In the process of searching the unbalance coefficient, an improved Sigmoid function is introduced to control the size of the step and angle changes, while the parameters of the improved Sigmoid function are adjusted online by using the fuzzy inference system, so that the changes of the step and angle of the algorithm can be varied in real time according to the feedback error signals, and it can converge quickly in the initial stage, but also improve the search accuracy of the algorithm in the later stage, thus the steady state error of the rotor is minimized. This method improves the rotor vibration suppression effect of PMa-BSynRM system. The effectiveness of the method in suppressing unbalance vibration of the rotor system is verified by simulation and experiment.

2. VIBRATION MECHANISM ANALYSIS

Due to machining defects and uneven materials, the center of mass and geometric center of the PMa-BSynRM rotor do not coincide, resulting in unbalanced rotor mass, and unbalanced vibration will be generated during the rotor rotation. The rotor motion equation is:

$$m\ddot{s} = F_m - F_L = (K_C i_s + K_M s) - F_L \tag{1}$$

where m is the rotor mass, F_m the electromagnetic force, F_L the external force (including the rotor weight and load), s the displacement in one direction (x direction or y direction), and i_s the current of the suspended winding in the x- and y-directions. K_C and K_M are the force-current constant and force-displacement constant of PMa-BSynRM, respectively.

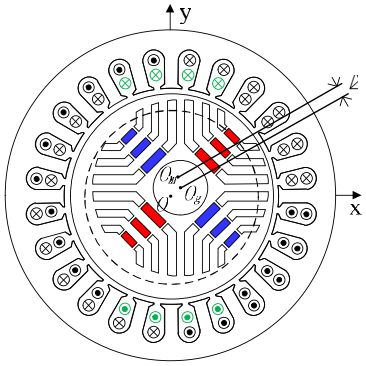

FIGURE 1. Unbalance vibration diagram of rotor.

As shown in Fig. 1, the geometrical center of the rotor is O_g; the mass center of the rotor is O_m; the geometrical center of the stator is O; and the coordinates of O_g in the x-y coordinate system centered on the stator center is (x, y). If the distance from the rotor mass center O_m to the rotor geometric center O_g is ε, when the rotor is rotating at the angular velocity ω, the unbalance force caused by the mass eccentricity is:

$$\begin{cases} F_x = m\omega^2[x + \varepsilon\cos(\omega t + \varphi)] \\ F_y = m\omega^2[y + \varepsilon\cos(\omega t + \varphi)] \end{cases} \tag{2}$$

where φ is the phase angle at which O_m deviates from O_g in the initial state.

In the case of mass eccentricity of the rotor, the motion equation of the rotor is:

$$\begin{cases} m\ddot{x} = F_x + K_C i_x + K_M x - F_{Lx} \\ m\ddot{y} = F_y + K_C i_y + K_M y - F_{Ly} \end{cases} \tag{3}$$

where F_{Lx} and F_{Ly} are the external force components of the rotor in the x- and y-directions, respectively.

3. DESIGN OF UNBALANCE VIBRATION SUPPERSSION CONTROLLER

Rotor shaft bending, wear, and other cause the rotor mass imbalance, resulting in that the center of the rotor is not the rotating center, and the rotor will be subjected to the unbalance force at the same frequency as the rotor speed, so that the unbalance vibration of the rotor system is generated. In this paper, an

unbalance vibration suppression method of PMa-BSynRM rotor system based on variable step size and variable angle search algorithm of fuzzy inference system is proposed.

3.1. Vibration Signal Processing

The vibration quantities of the rotor are identified by Fourier series, and the cosine and sine signals are obtained, respectively, with cosine coefficients a_x, a_y and sine coefficients b_x, b_y. For the two-degree-of-freedom PMa-BSynRM system, one end of the rotor is supported by a ball bearing, and the other end is suspended by suspension force, so it is sufficient to consider only the same-frequency vibration of the suspended end. The rotor homodyne vibration signals in the x- and y-directions are written in the form of Fourier series as:

$$\begin{cases} x(t) = A_0 + a_x \cos(\omega t) + b_x \sin(\omega t) \\ y(t) = A_1 + a_y \cos(\omega t) + b_y \sin(\omega t) \end{cases} \tag{4}$$

where $A_0 = {}^1\!/_{2\pi} \int_{-\pi}^{\pi} x(t)dtA_1 = {}^1\!/_{2\pi} \int_{-\pi}^{\pi} y(t)dt$.

After discretization, the cosine coefficients a_x a_y and sine coefficients b_x, b_y on one side of the suspension end are obtained as:

$$\begin{cases} a_x(k) = \frac{2}{N} \sum\limits_{k=1}^{N} x(kT_s) \cos(\omega k T_s) \\ b_x(k) = \frac{2}{N} \sum\limits_{k=1}^{N} x(kT_s) \sin(\omega k T_s) \\ a_y(k) = \frac{2}{N} \sum\limits_{k=1}^{N} y(kT_s) \cos(\omega k T_s) \\ b_y(k) = \frac{2}{N} \sum\limits_{k=1}^{N} y(kT_s) \sin(\omega k T_s) \end{cases} \tag{5}$$

where $N = 2\pi/(\omega T_s)$, T_s is the sampling period.

Then, the amplitudes of the unbalanced vibration signals in the x- and y-directions are:

$$\begin{cases} A_x(k) = \sqrt{a_x(k)^2 + b_x(k)^2} \\ A_y(k) = \sqrt{a_y(k)^2 + b_y(k)^2} \end{cases} \tag{6}$$

where A_x and A_y are the vibration amplitudes in the x- and y-directions, respectively.

Therefore, the amplitude of the unbalanced vibration signal on the suspended side of the motor is expressed as:

$$A(k) = \sqrt{A_x(k)^2 + A_y(k)^2} \tag{7}$$

$A(k)$ represents the unbalanced vibration amplitude of the unbalanced rotor. When $A(k)$ is greater than a certain value A_o, the algorithm is started. This value is too large to cause the algorithm to suppress the vibration effect which is not obvious, and if it is too small, the algorithm will converge slowly. Therefore, the algorithm selects 20% of the unbalanced vibration amplitude as the target vibration amplitude.

3.2. Calculating Compensation Current

The variable-step-variable-angle search algorithm causes the compensator to generate a compensating current to counteract the equivalent unbalance force. This method belongs to a rotor displacement minimization control method where the generated compensation current will rotate the unbalanced rotor as much as possible around its geometrical axis. Therefore, the compensation current needs to be calculated based on the rotor system dynamics model. In fact, due to the existence of unbalanced mass and limitations of the algorithm, the synchronous vibration of the rotor system cannot be completely suppressed, which means that the rigid rotor cannot be absolutely rotated around its geometrical axis, so that x, y should be a very small non-zero constant, and then, $\ddot{x}$ and $\ddot{y}$ are zero. According to Equation (3), we can get the compensating currents in the x- and y-directions i_{c-x} and i_{c-y}:

$$\begin{cases} i_{c-x} = -\frac{m\omega^2 \varepsilon \cos(\omega t+\varphi)}{K_C} + \frac{F_{Lx} - (m\omega^2 + K_M)x}{K_C} \\ i_{c-y} = -\frac{m\omega^2 \varepsilon \cos(\omega t+\varphi)}{K_C} + \frac{F_{Ly} - (m\omega^2 + K_M)y}{K_C} \end{cases} \tag{8}$$

Without considering the influence of external interference force on rotor vibration, the identification coefficients α_X, β_X are defined as:

$$\begin{cases} \alpha_X = -\frac{m}{K_C} \varepsilon \cos(\omega t + \varphi) \\ \beta_X = -\frac{m}{K_C} \varepsilon \cos(\omega t + \varphi)] \end{cases} \tag{9}$$

The relationship between the identification coefficients and the current can be obtained:

$$\begin{cases} i_{c-x} = \omega^2 \alpha_X \\ i_{c-y} = \omega^2 \beta_X \end{cases} \tag{10}$$

3.3. Variable Step Size and Angle Search Algorithm

According to the above deduction, the appropriate identification coefficients are calculated, and the compensation currents of the unbalanced vibration are obtained. Then, the compensation currents are fed back to the control system to complete the vibration compensation of the unbalanced rotor. In this paper, variable step size and variable angle search algorithm is used to search the identification coefficients. The variable step size and variable angle search algorithm is described below.

As in Fig. 2, set the O point in the two-dimensional plane as the target value, that is, when the coordinate corresponding to the identification coefficient is the O point coordinate, the vibration amplitude of the rotor is the target vibration amplitude. When the initial vibration value is greater than the set vibration target value, the algorithm starts. In each subsequent step, changing modes and angles of vector, a new vector is obtained. Through the superposition of the vectors, the identification coefficient approaches the target point O. Finally, the algorithm converges to the target point with changing step size and angle. The step size of change and angle of change are obtained by the

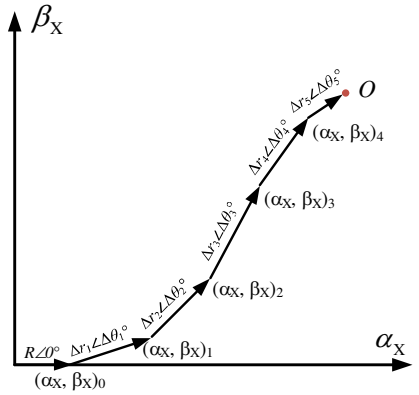

FIGURE 2. Variable step size and variable angle search process diagram.

improved Sigmoid function. The calculation methods of Δr_k, $\Delta\theta_k$ are:

$$\begin{cases} \Delta\theta_k = \theta_k - \theta_{k-1} = \frac{\beta_1}{1+e^{-\alpha_1\varepsilon(k)^2}} + \gamma_1 \\ \Delta r_k = r_k - r_{k-1} = \frac{\beta_2}{1+e^{-\alpha_2\varepsilon(k)^2}} + \gamma_2 \end{cases} \tag{11}$$

Parameter α controls the shape of the function; parameter β controls the amplitude of the function; parameter γ is the control parameter of algorithm convergence speed. The selection value of parameters β and γ is very important for the various stages in the convergence of the algorithm. In the early stage of convergence, the rotor vibrates violently, and a larger step factor is needed to strengthen the tracking ability. In the late stage of convergence, a smaller step factor is needed to reduce the steady state error and improve the convergence accuracy. Therefore, combining the fuzzy theory with adaptive theory, the curve adjustment parameters β and γ in the improved Sigmoid function model are adjusted by the fuzzy inference system, which adopts the first-order Takagi-Sugeno (TS) fuzzy inference machine.

The detailed search processes of the algorithm are as follows.

Figure 3 shows the flowchart of variable step size and variable angle search algorithm. Set the initial vector $\mathbf{r} = r\angle\theta°$, where $r = R$, $\theta_0 = 0$, this time, $(\alpha_X, \beta_X) = (R, 0)$. If the vibration value $A(0)$ is greater than the target vibration value A_o, the algorithm starts. When $k = 1$, $r_1 = r + \Delta r_1$, $\theta_1 = \theta + \Delta\theta_1$, let $\Delta\mathbf{r_1} = \Delta r_1\angle\Delta\theta_1°$, then get the superposition vector $\mathbf{r_1} = \mathbf{r} + \Delta\mathbf{r_1}$. The identification coefficient vector is $(\alpha_X, \beta_X)_1 = \mathbf{r_1}$. Determine if $A(1)$ is greater than A_o, and if meeting the conditions, continue to iterate, and get $(\alpha_X, \beta_X)_2$, $(\alpha_X, \beta_X)_3$, $(\alpha_X, \beta_X)_4$, etc. When the calculated vibration amplitude gets closer and closer to the target value, according to the rules of the fuzzy inference machine, Δr_k and $\Delta\theta_k$ will decrease or become negative, and finally search to the target point O with a small step size.

3.4. TS Fuzzy Inference Machine

The amount of change in step size and angle in the search algorithm is affected by the error e, the primary change in error de, and the secondary change in error d^2e. Therefore, the curve

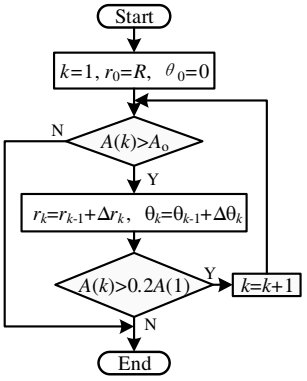

FIGURE 3. Flowchart of variable step size and variable angle search algorithm.

adjustment parameters β_1, β_2 and γ_1, γ_2 in the formula of variable angle and variable step size are related to e, de, and d^2e. Select e, de, and d^2e as system inputs, and β_1, β_2, and γ_1, γ_2 as system outputs. e has three fuzzy sets: small (S), medium (M), and large (L), de and d^2e have two fuzzy sets: negative (N) and positive (P). The membership function adopts cosine function to achieve ambiguity, as shown in Fig. 4. The outputs of the system β_1, β_2 and γ_1, γ_2 are also divided into three levels: small (S), medium (M), and large (L).

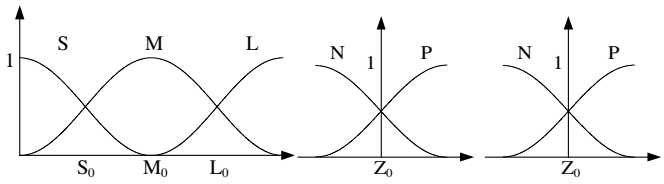

FIGURE 4. Membership function.

The fuzzy inference system adopts a first-order TS fuzzy inference machine, which makes R_i represent the i-th rule of the fuzzy system. The first-order fuzzy conditional statement is as follows:

R^i: If x_1 is A_1^i and ..., and x_n is A_n^i, then $y^i = a_0^i + a_1^i x_1 + \ldots + a_n^i x_n$, where x_n is the n-th input variable in the i-th rule, $n = 1, 2, 3 \ldots k$. A_n^i is the fuzzy set corresponding to x_n in the i-th rule, y^i the output of the i-th rule, and a_n^i the parameter corresponding to the x_n of the i-th rule.

As shown in Fig. 5, the input of the fuzzy inference machine is e, de, and d^2e. By blurring e, de, and d^2e, the output is obtained according to the output function $u^j = a_0^j + a_1^j e + a_2^j de + a_3^j d^2e$.

Figure 6 shows the structure of TS fuzzy inference machine. The first column inputs the actual signal; the second column is the blur layer; the third and fourth columns are fuzzy reasoning; and the fifth column gets the clear output. Input e has 3 fuzzy subsets, and input de and d^2e have 2 fuzzy sets, corresponding to 12 fuzzy rules. Each rule corresponds to 1 output, and 12 outputs are processed into a total output u, four groups of fuzzy inference system outputs β_1, β_2, γ_1, γ_2, respectively.

The fuzzy rules of TS fuzzy inference machine are shown in Table 1. The first order TS fuzzy inference system uses the weighted average method to process the output of each fuzzy

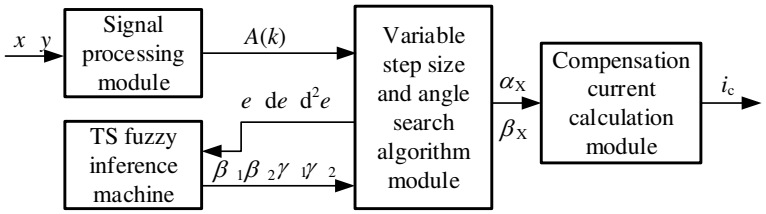

FIGURE 5. Unbalance force suppression module.

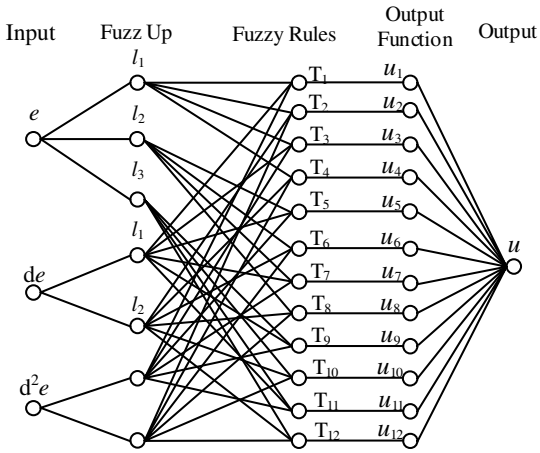

FIGURE 6. The structure of fuzzy inference machine.

TABLE 1. Fuzzy control rules.

Inputs			Outputs			
e	de	d^2e	β_1	β_2	γ_1	γ_2
S	N	N	S	S	S	S
S	N	P	S	S	S	S
S	P	N	S	S	S	S
S	P	P	S	S	S	M
M	N	N	M	M	S	M
M	N	P	M	M	M	M
M	P	N	M	M	M	M
M	P	P	M	M	M	M
L	N	N	L	M	L	M
L	N	P	L	L	L	L
L	P	N	L	L	L	L
L	P	P	L	L	L	L

rule and finally gets the total output, where the weight of each rule is the product of the affiliation of the three variables in the rule.

4. ANALYSIS OF SIMULATION RESULTS

The research object of this paper is PMa-BSynRM. In order to verify the effectiveness of the compensator based on variable step size and variable angle search algorithm on vibration suppression of PMa-BSynRM rotor system, a simulation model of the control system is established in MATLAB. The simulation in this paper detects the displacement signal of the rotor at the suspended end. Fig. 7 shows the PMa-BSynRM rotor vibration suppression control block diagram based on variable step size and variable angle search algorithm, and the simulation platform is built according to the control block diagram.

In this paper, the rotor displacement signal maps based on the conventional extended Kalman filter are compared with the rotor displacement signal maps based on the adaptive filter with variable step size and variable angle search algorithm.

The rotor vibration signal is a sine wave signal with the same frequency as the rotor speed. In this simulation, the sine wave signal is superimposed into the displacement signal of the rotor in the x- and y-directions to simulate the unbalanced vibration of the rotor. When the rotor speed is 3,000 r/min, the superimposed sine wave signal frequency is 50 Hz, and amplitude is 50 µm.

According to the settings of the simulation system, the rotor unbalance vibration control is carried out when the system runs for 0.3 s. Fig. 8 compares the waveforms of the rotor displacement in the x direction under the vibration suppression method proposed in this paper with those under the extended Kalman filter.

As can be seen from Fig. 8, under the vibration suppression method proposed in this paper, after 0.3 s, the rotor vibration suppression control makes the rotor vibrate irregularly. The rotor vibration waveform is changed again according to the sinusoidal law, and the rotor vibration amplitude is 10 µm after 0.12 s. Under the control of the extended Kalman filter, the algorithm converges in the x direction in about 0.15 s, and the vibration amplitude stabilizes at 12 µm.

Figure 9 compares the rotor displacement waveforms in the y direction for both methods. Since the air gap of the motor is 0.5 mm, the starting position of the displacement waveform in the y direction is -0.5 mm. Under the vibration suppression method proposed in this paper, the amplitude is stabilized at 10 μm after 0.12 s, and under the control of the extended Kalman filter, the amplitude is stabilized at 13 µm after 0.15 s.

Comparing the vibration amplitudes before and after vibration suppression control, it can be seen that the amplitude after control is about 20% of the amplitude before the control, which is consistent with the setting in the controller. It can be seen that the vibration suppression control method proposed in this paper is superior to that of the vibration suppression method based on the extended Kalman filter.

When the rotor speed is 6,000 r/min, the frequency of the corresponding sine wave signal is 100 Hz, and the faster the speed is, the greater the influence of the rotor mass imbalance is on its rotation, which is reflected in the simulation and increases the amplitude of the sine wave superimposed in the displacement signal, and the amplitude is set to 100 µm.

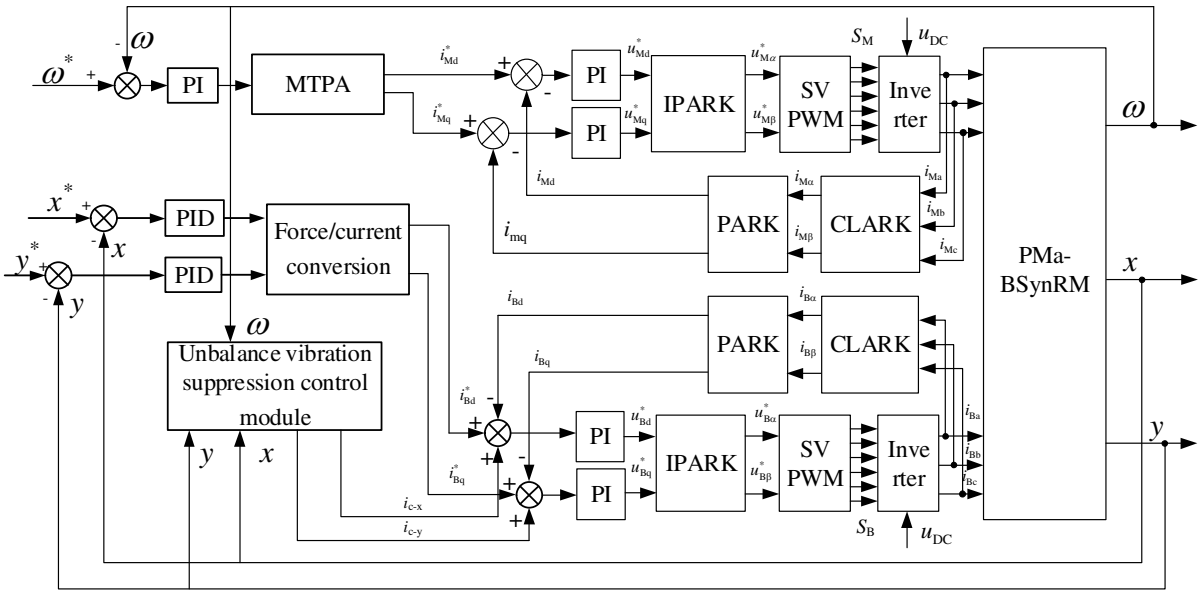

FIGURE 7. Vector control block diagram of the PMa-BSynRM.

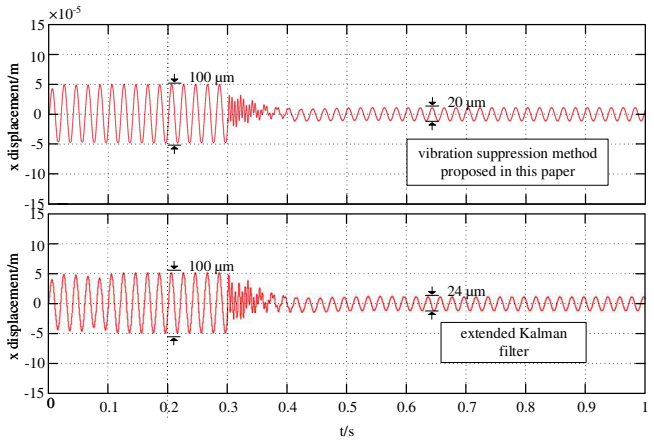

FIGURE 8. Comparison of rotor displacement waveforms in the x direction under the two control methods (3 000 r/min).

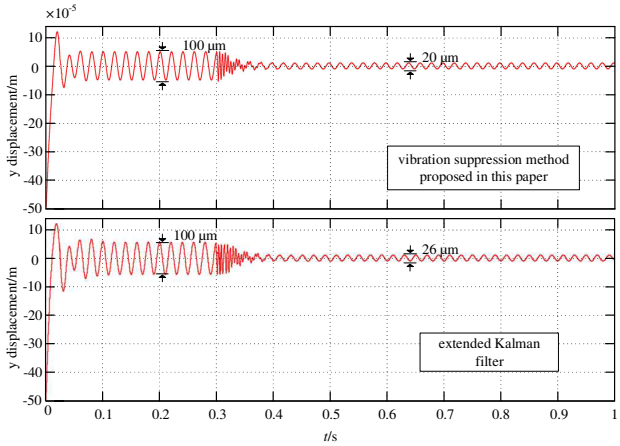

FIGURE 9. Comparison of rotor displacement waveforms in the y direction under the two control methods (3 000 r/min).

Figure 10 shows a comparison of the waveforms of the rotor displacement in the x direction at 6,000 r/min of the motor with the two methods. Under the vibration suppression method proposed in this paper, the algorithm converges at 0.15 s, and the amplitude in the x direction is stabilized at 20 μm, about 20% of the initial value. Under the control of the extended Kalman filter, it can be seen that the algorithm converges after 0.2 s, and the amplitude in the x direction is 26.5 μm.

Figure 11 shows a comparison of the waveforms of the rotor displacement in the y direction at 6000 r/min of the motor with the two methods. Under the vibration suppression method proposed in this paper, the algorithm converges at 0.15 s and the amplitudes in y direction is stabilized at 20 μm, about 20% of the initial value. Under the control of the extended Kalman filter, the algorithm converges after 0.2 s, and the amplitude in the y direction is 29 μm.

The method proposed in this paper has obvious advantages in the aspects of rapidity and high efficiency. It is almost independent of the initial state value. The simulation results show that the rotor vibration suppression controller based on variable step size and variable angle search algorithm has good vibration suppression effect at different speeds.

5. EXPERIMENTAL ANALYSIS

In this section, in order to verify the effectiveness of rotor vibration suppression, an experimental platform of PMa-BSynRM is designed to verify the proposed unbalance vibration suppression control strategy.

The experimental equipment, as shown in Fig. 12, mainly includes displacement interface circuit, DSP controller minimum system, DC power supply, eddy current sensor, power driver board, AC power supply, personal computer (PC), etc.

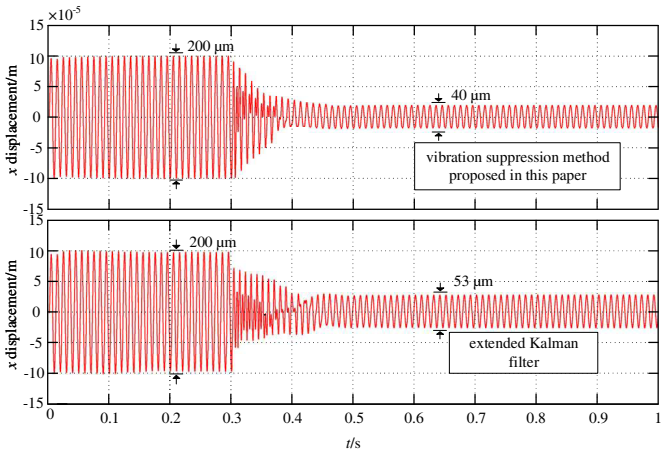

FIGURE 10. Comparison of rotor displacement waveforms in the x direction under the two control methods (6 000 r/min).

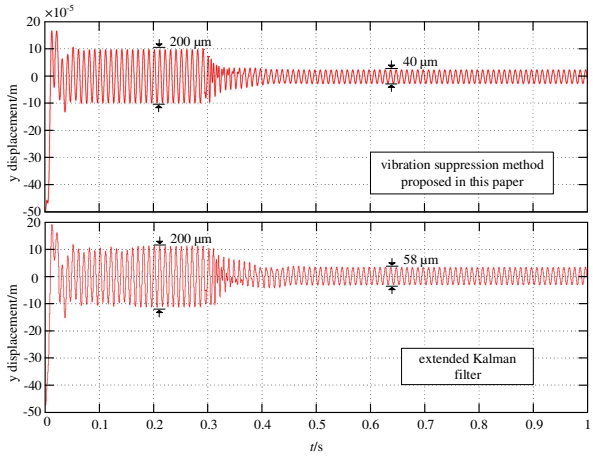

FIGURE 11. Comparison of rotor displacement waveforms in the y direction under the two control methods (6 000 r/min).

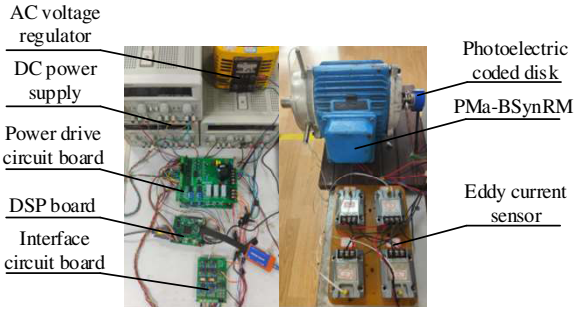

FIGURE 12. Experimental platform.

The controller is TMS320F28335 with an interrupt frequency of 10 kHz. The torque vector control algorithm and suspension force control algorithm are implemented simultaneously during the interrupt process. The power device is PS21965; the upper power drive circuit board supplies power to the torque winding; and the lower power drive circuit board supplies power to the suspension force winding. The outputs of the two power driver boards are generated by the Hall current sensors to generate sampling current and then adjusted by the interface circuit board.

The DSP converts the sampled analog signals into digital signals for data processing. The torque control system adopts maximum torque per ampere (MTPA) control, and the unbalance vibration control adopts minimum displacement control criterion. The eddy current sensor detects the real-time position information of the rotor through the interface circuit board, sends it to the analog-to-digital converter (ADC) port on the digital signal processing (DSP) for data acquisition, and performs signal processing through the controller. The unbalanced vibration of the rotor is detected by the eddy current sensor, and the error signal is obtained by the difference with the reference balance position signal through the displacement interface circuit. The compensator based on the variable step size and variable angle search algorithm searches the identification coefficient according to the error signal, calculates the compensation current, and finally completes the vibration suppression control of the rotor.

The prototype of this experiment is a two-degree-of-freedom PMa-BSynRM, where one end is supported by a three-degree-of-freedom aligning ball bearing, and the other end is equipped with an auxiliary bearing, which can realize two-degree-of-freedom suspension. The basic parameters of the prototype are shown in Table 2.

TABLE 2. Main parameters of PMa-BSRM.

Quantity	Value	Quantity	Value
n	0–6 000 r/min	δ_0	0.5 mm
U_N	220 V	ψ_0 (Wb)	0.0359 Wb
P_N	1.1 kW	L_{Md}/L_{Mq}	11.2/66.2 mH
P_M/P_B	2/1	L_B	2.34 mH
m	1.6 kg	*Cost*	4 × 300 $

The experiments of unbalanced vibration reduction control were carried out at 3,000 r/min and 6,000 r/min of PMa-BSynRM. When the motor is running at 3,000 r/min and 6,000 r/min, the unbalanced vibration frequency of the rotor is 50 Hz and 100 Hz, respectively. When the system is not controlled for vibration suppression, as can be seen from Fig. 13(a), as the rotor speed is 3 000 r/min, the amplitudes of the rotor in the x- and y-directions are 11 μm and 12 μm, respectively. As can be seen from Fig. 13(b) when the rotor speed is 6 000 r/min, the amplitudes in the x- and y-directions of the rotor are 19 μm and 20.5 μm, respectively. Fig. 14(a) and Fig. 14(b) show the trajectory of the rotor at rotor speeds of 3,000 and 6,000 r/min. With the increase of the rotational speed, the unbalanced vibration of the rotor increases obviously, so it is necessary to suppress the vibration of the system.

As shown in Fig. 15, after the vibration suppression control of the rotor is carried out by the compensator based on the variable step size and variable angle search algorithm, the rotor vibration amplitudes in the x- and y-directions decrease significantly. As can be seen from Fig. 15(a), when the rotor speed is 3,000 r/min, the rotor amplitudes decrease to 2.75 μm in the

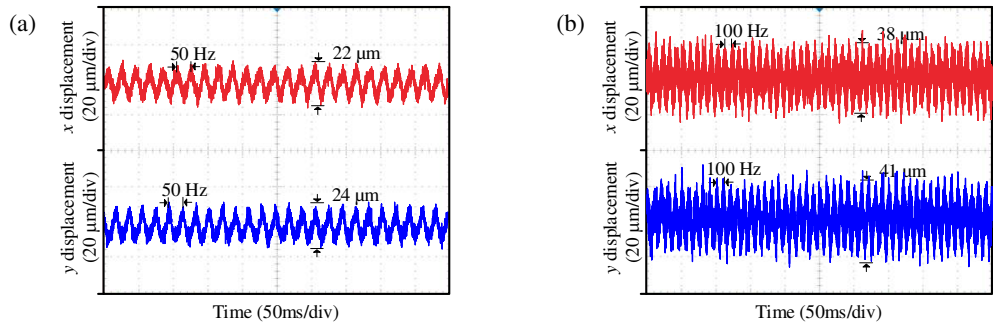

FIGURE 13. Displacement waveform of rotor without vibration suppression. (a) 3 000 r/min. (b) 6 000 r/min.

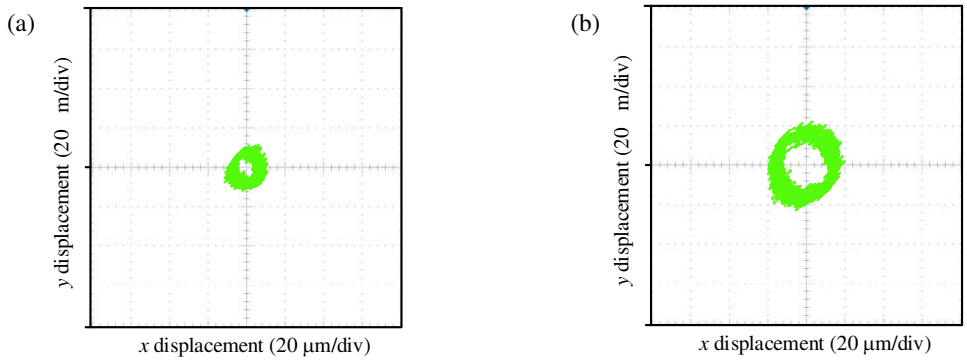

FIGURE 14. Rotor motion trajectory without vibration suppression. (a) 3 000 r/min. (b) 6 000 r/min.

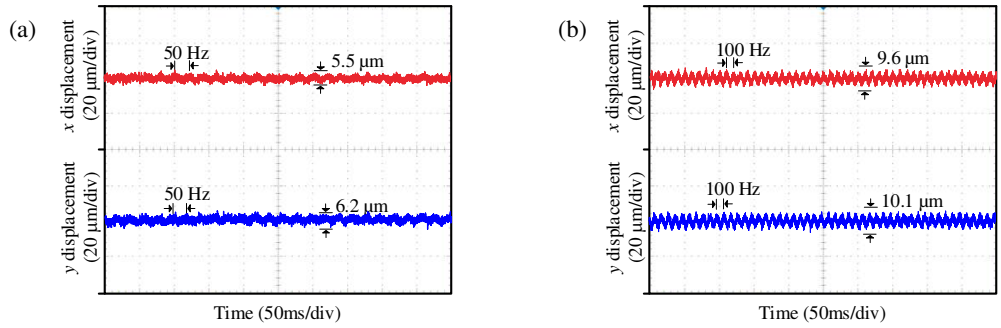

FIGURE 15. Displacement waveform of rotor under vibration suppression control. (a) 3 000 r/min. (b) 6 000 r/min.

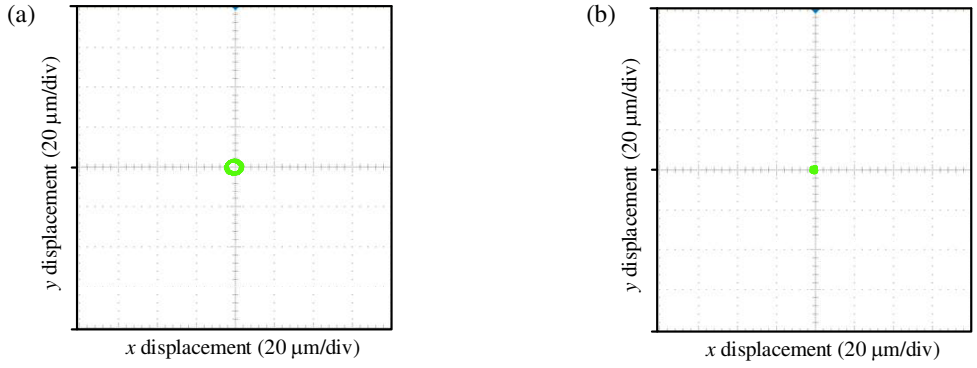

FIGURE 16. Rotor motion trajectory under vibration suppression control. (a) 3 000 r/min. (b) 6 000 r/min.

TABLE 3. Amplitudes before and after control at 3,000 and 6,000 r/min.

Amplitude in the x direction (3 000 r/min)		Amplitude in the y direction (3 000 r/min)	
before	after	before	after
11 μm	2.75 μm	12 μm	3.1 μm
Amplitude in the x direction (6,000 r/min)		Amplitude in the y direction (6,000 r/min)	
before	after	before	after
19 μm	4.8 μm	20.5 μm	5.05 μm

x direction and 3.1 μm in the y direction. The amplitudes are reduced by 75% and 74.2%, respectively. As can be seen from Fig. 15(b), when the rotor speed is 6,000 r/min, the rotor amplitudes decrease to 4.8 μm in the x direction and 5.05 μm in the y direction. The amplitudes are reduced by 74.7% and 75.4%. Fig. 16(a) and Fig. 16(b) show the trajectory of the rotor at rotor speeds of 3,000 and 6,000 r/min after vibration suppression control, respectively.

Table 3 shows the amplitudes of the rotor before and after control at 3,000 and 6,000 r/min, and it summarizes the results of the above experiments.

The experimental results show that the rotor vibration suppression controller based on the variable step size and variable angle search algorithm can complete the vibration suppression quickly, and the steady-state error is small. In addition, the step size and angle of the algorithm can be adjusted adaptively according to the error signal, which can meet the requirements of the step size and angle in different convergence stages under different rotor speeds, so that PMa-BSynRM has higher working accuracy.

6. CONCLUSION

In this paper, an adaptive vibration suppression method based on variable step size and angle search algorithm is proposed for unbalance vibration suppression control of PMa-BSynRM rotor system. The conclusions are as follows:

1. The vibration mechanism of PMa-BSynRM rotor unbalance vibration is analyzed, which provides a theoretical basis for the acquisition of compensation current.
2. The coefficients of the compensation current are searched with the variable step size and variable angle search algorithm, and the step and angle of the vectors in the searching process are adaptively adjusted using the improved Sigmoid function and fuzzy inference system, which has a better adaptivity, so that the algorithm can be more quickly and accurately converged to the target value and has a certain degree of anti-interference.
3. The experimental results show that the proposed method reduces the rotor amplitude by about 75%, is less affected by the initial amplitude of the rotor vibration, and has excellent vibration suppression performance. This method provides a guarantee for the application of PMa-BSynRM in high-speed and high-precision occasions.

ACKNOWLEDGEMENT

This project was sponsored in part by the National Natural Science Foundational of China (62273168)

REFERENCES

[1] Zhu, H. and Y. Shi, "Displacement self-sensing control of permanent magnet assisted bearingless synchronous reluctance motor based on least square support vector machine optimized by improved NSGA-II," *IEEE Transactions on Industrial Electronics*, Vol. 71, No. 2, 1201–1211, Feb. 2024.

[2] Pei, T., D. Li, J. Liu, J. Li, and W. Kong, "Review of bearingless synchronous motors: Principle and topology," *IEEE Transactions on Transportation Electrification*, Vol. 8, No. 3, 3489–3502, Sep. 2022.

[3] Hua, Y., H. Zhu, M. Gao, and Z. Ji, "Multiobjective optimization design of permanent magnet assisted bearingless synchronous reluctance motor using NSGA-II," *IEEE Transactions on Industrial Electronics*, Vol. 68, No. 11, 10 477–10 487, Nov. 2021.

[4] Ji, Z., H. Zhu, Y. Xu, and M. Wu, "Optimization design of permanent magnet assisted single winding bearingless synchronous reluctance motor," *IEEE Transactions on Applied Superconductivity*, Vol. 30, No. 4, 1–5, Jun. 2020.

[5] Islam, M. Z., A. Arafat, and S. Choi, "Design of five-phase bearingless permanent magnet assisted synchronous reluctance motor for high speed applications," in *2018 IEEE Energy Conversion Congress and Exposition (ECCE)*, 4419–4424, Portland, OR, USA, 2018.

[6] Peng, C., M. Zhu, K. Wang, Y. Ren, and Z. Deng, "A two-stage synchronous vibration control for magnetically suspended rotor system in the full speed range," *IEEE Transactions on Industrial Electronics*, Vol. 67, No. 1, 480–489, Jan. 2020.

[7] Wang, X. and H. Zhu, "Vibration compensation control of BPMSM with dead-time effect based on adaptive neural network band-pass filter," *IEEE Transactions on Power Electronics*, Vol. 37, No. 6, 7145–7155, Jun. 2022.

[8] Shi, J. and H. Zhu, "Control study for compensating rotor vibration of four-DOF six-pole hybrid magnetic bearings based on variable step size LMS algorithm," *IEEE Journal of Emerging and Selected Topics in Power Electronics*, Vol. 11, No. 2, 1616–1626, Apr. 2023.

[9] Zheng, S., Q. Chen, and H. Ren, "Active balancing control of AMB-rotor systems using a phase-shift notch filter connected in parallel mode," *IEEE Transactions on Industrial Electronics*, Vol. 63, No. 6, 3777–3785, Jun. 2016.

[10] Xu, Z. and C. Zhu, "Vibration control of an active magnetic bearings flexible rotor system based on adaptive recursive least square algorithm," in *2021 24th International Conference on Electrical Machines and Systems (ICEMS)*, 1948–1952, Gyeongju, Korea, 2021.

[11] Mao, B. and H. Zhu, "Unbalance vibration suppression control of PMa-BSynRM based on total least square adaptive filtering algorithm," *IEEE Journal of Emerging and Selected Topics in Power Electronics*, Vol. 11, No. 6, 5798–5808, Dec. 2023.

[12] Gong, L. and C. Zhu, "Vibration suppression for magnetically levitated high-speed motors based on polarity switching tracking filter and disturbance observer," *IEEE Transactions on Industrial Electronics*, Vol. 68, No. 6, 4667–4678, Jun. 2021.

[13] Zhang, P. and C. Zhu, "Vibration control of base-excited rotors supported by active magnetic bearing using a model-based compensation method," *IEEE Transactions on Industrial Electronics*, Vol. 71, No. 1, 261–270, Jan. 2024.

[14] Yang, Z., J. Jia, X. Sun, and T. Xu, "A fuzzy-ELADRC method for a bearingless induction motor," *IEEE Transactions on Power Electronics*, Vol. 37, No. 10, 11 803–11 813, Oct. 2022.

[15] Zad, H. S., T. I. Khan, and I. Lazoglu, "Design and adaptive sliding-mode control of hybrid magnetic bearings," *IEEE Transactions on Industrial Electronics*, Vol. 65, No. 3, 2537–2547, Mar. 2018.

[16] Li, Y. and H. Zhu, "Three-vector model predictive suspension force control for bearingless permanent magnet slice motor," *IEEE Transactions on Power Electronics*, Vol. 38, No. 7, 8282–8290, Jul. 2023.